ENVIRONMENTAL RESEARCH
LETTERS

PURPOSE-LED PUBLISHING™ Part of the ENVIRONMENTAL RESEARCH SERIES

LETTER • OPEN ACCESS

Drylands face potential threat of robust drought in the CMIP6 SSPs scenarios

To cite this article: Hongwei Li *et al* 2021 *Environ. Res. Lett.* **16** 114004

ENVIRONMENTAL RESEARCH
LETTERS

OPEN ACCESS

RECEIVED
18 June 2021

ACCEPTED FOR PUBLICATION
30 September 2021

PUBLISHED
14 October 2021

LETTER

Drylands face potential threat of robust drought in the CMIP6 SSPs scenarios

Hongwei Li[1,2], Zhi Li[1,*], Yaning Chen[1,*], Yanyun Xiang[1,2], Yongchang Liu[1,2], Patient Mindje Kayumba[1,2] and Xiaoyang Li[1,2]

[1] State Key Laboratory of Desert and Oasis Ecology, Xinjiang Institute of Ecology and Geography, Chinese Academy of Sciences, Urumqi 830011, People's Republic of China
[2] University of Chinese Academy of Sciences, Beijing 100049, People's Republic of China
[*] Authors to whom any correspondence should be addressed.

E-mail: liz@ms.xjb.ac.cn and chenyn@ms.xjb.ac.cn

Keywords: global warming, drought, drylands, CMIP6, SSPs

Abstract

In an increasingly globalized and warming world, drought can have devastating impacts on regional agriculture, water resources, and the ecological environment. Reliable prediction of future drought changes is especially important within the context of rapid warming. However, the extent and future trends of drought changes are variable and incomplete in the CMIP6 forcing scenarios. Based on the CMIP6 data, we chose the standardized precipitation-evapotranspiration index to predict future global drought. The results show that when emissions increase under the three shared socioeconomic pathway (SSP) scenarios (SSP126, SSP245 and SSP585), the global climate environment becomes drier and drought grow more severe and longer-lasting. Regions already classified as arid will suffer even more severe drought under high-emission SSPs. Specifically, 36.2% of global land will experience increased drought under SSP126, including 67.0% of regions designated as arid, with droughts intensifying significantly. Under SSP585, 68.3% of global land will suffer increased drought, with 93.2% of the arid regions experiencing significant drought intensification. Furthermore, the global duration of drought is estimated to be 4.4 months, 5.7 months, and 8.6 months for the time periods 1960–2000, 2021–2060, and 2061–2100, respectively. Notably, for the SSP585 scenario, regions that are already arid may become universally drought-stricken by the late 21st century. The most severe aridification trends may occur in the arid regions of Australia, Middle East, South Africa, Amazon basin, North Africa, Europe, and Central Asia. Additionally, Europe and the Amazon River Basin are also facing the threat of future drought. Increased aridification will put these regions and countries at risk of further land and ecological degradation, as well as increased poverty. The results of this study have far-ranging implications not only for how we deal with the impacts of climate warming-induced drought disaster, but also for how these impacts affect socio-economic and ecological security.

1. Introduction

According to the statistical results of the International Disaster Database (EM-DAT 2021), the share of economic losses caused by drought is as high as 59% of all climate disaster economic losses. The impacts of drought involve many fields on the agricultural production (Webber *et al* 2018), economic development (Ding *et al* 2011), social stability (Wang *et al* 2015, 2019, Yang *et al* 2021), water resources management (Zhang *et al* 2015), and local ecosystem functioning (Van Dijk *et al* 2013, Staal *et al* 2020). Statistics show that between 1900 and 2021, drought caused 11.73 million deaths and affected more than 2.7 billion people (EM-DAT 2021). It is worth noting that three-quarters of the expansion of arid regions is occurring in poor and technologically under-developed countries (Huang *et al* 2017). The increase in aridification will put these regions and countries at risk of further land degradation and increased poverty. Therefore, it is imperative to study the changing trends of anticipated future drought events to prevent the world's most

vulnerable nations from sliding deeper into poverty. How will climatic aridity change in future as a consequence of the ongoing accumulation of greenhouse gases?

Drought is slower and more complicated in both its occurrence and development process, compared to other natural disasters. Drought indexes are often used to describe long-term changes of drought events, and a standardized precipitation evapotranspiration index (SPEI) based on precipitation and potential evapotranspiration (PET) can reflect deficit of water in a changing environment. The primary approach uses the Thornthwaite evapotranspiration formula, neglecting the variations of solar and infrared radiation, humidity and wind speed (Sheffield *et al* 2012, Dai 2013). In this way, the role of air temperature is exaggerated (Zhang *et al* 2016, Li *et al* 2017), and evapotranspiration in arid and semi-arid regions may be underestimated, while in wet regions may be overestimated (Donohue *et al* 2010, Van Der Schrier *et al* 2011, Chen and Sun 2015). The Food and Agriculture Organization of the United Nations (FAO) recommends the Penman–Monteith equation, which incorporates the effects of heat and dynamics on evapotranspiration such as changes in temperature, solar and infrared radiation, humidity and wind speed (Sheffield *et al* 2012, Trenberth *et al* 2014). It is now recognized that one should apply physically based approaches to investigate the future global drought changes.

Projected changes in the long-term aridity can be assessed by directly interrogating the climate model output. In terms of predictions of future climate change, previous investigations showed that CMIP6 is more reliable and stable than CMIP5 (Chen *et al* 2020, Nie *et al* 2020). This is because CMIP6 has adopted more reasonable shared socioeconomic pathways (SSPs) by sharing policy assumptions to work in coordination with RCPs compared to CMIP5 (Ritchie and Dowlatabadi 2017) (Anon 2019).

CMIP6 has improved performance in many drought-related aspects, from predicting ecosystem processes (e.g. leaf area index) to hydrological processes such as runoff, terrestrial water storage, and surface energy allocation (Cook *et al* 2020). Simulations of historical surface temperature extremes show a better agreement of CMIP6 models with ERA5 than CMIP5 models (Thorarinsdottir *et al* 2020), as the CMIP6 models are better at capturing the observed global and regional extreme temperature patterns in terms of improved partial higher horizontal resolution and representation of weather processes. Moreover, compared to CMIP5, CMIP6 exhibits a general improvement in simulating extreme climates and their trend patterns for most terrestrial regions in extreme climate studies (Agel and Barlow 2020, Chen *et al* 2020, Di Luca *et al* 2020, Kim *et al* 2020, Srivastava *et al* 2020). Additionally, CMIP6 is also more consistent with the most recent reference estimate for global energy balance (Wild 2020). Based on CMIP6 simulations, several droughts predictions have been conducted at global and regional (China, South Asia) scales (Cook *et al* 2020, Ukkola *et al* 2020, Zhai *et al* 2020), with strong drought trends being found in many regions. Previous research findings have shown the strong ability of CMIP6 to capture historical drought features (Su *et al* 2020). Notably, the most previous prediction studies have focused on average/extreme temperatures or precipitation, neglecting the long-term variation in drought characteristics. Few studies have been conducted at the global scale, considering the latest CMIP6 and changes in the duration, frequency, and intensity of drought events.

Considering the improvements in CMIP6, the new Global Climate Model (GCM) and SPEI is more capable of correctly predicting future drought event characteristics. The aim of this paper is to investigate drought characteristics based on the outputs of nine CMIP6 models under three high, medium and low scenarios (SSP126, SSP245, SSP585). In this study, the CMIP6 GCMs behave been resampled to ensure that all models have the same horizontal resolution, then evaluated based on observed data, and finally predicted future changes in drought characteristics across the globe for the time periods 2021–2060 (near term), and 2061–2100 (long term).

2. Data and methods

2.1. Datasets

2.1.1. Observation-based data

The monthly records of temperature, precipitation and other climatic factors for the observation data are from the latest Climate Research Unit dataset (CRU TS v4.04). According to the official data description for the CRU, these climatic factors is generated using angular-distance weighting interpolation based on over 4000 weather stations around the world, and its PET data are calculated based on the Penman–Monteith method (Harris *et al* 2020).

2.1.2. Climate model data

In this study, we used data from nine GCMs under the latest CMIP6 data. The shared SSPs analyzed were SSP126, SSP245, and SSP585, the same variant label 'r1i1p1f1' be used for all data, nine publicly accessible models were used (ACCESS-CM2, ACCESS-ESM1-5, CanESM5, FIO-ESM-2-0, IPSL-CM6A-LR, MRI-ESM2-0,GFDL-ESM4, INM-CM5-0 and MIROC6).

2.2. Research methods

2.2.1. Drought indicator

The SPEI was first proposed by Vicente-Serrano *et al* (2010) to describe conditions based on the deviation of the differences between precipitation and PET from the mean state (Vicente-Serrano *et al* 2010). In this study, SPEI values on a 12 month time-scale

are used to characterize drought in different climatic regions around the world. The steps used in the calculation are given below.

First, the FAO Penman–Monteith equation was employed to calculate PET for the period 1950–2100 (Allen *et al* 1998), as follows:

$$\mathrm{PET} = \frac{0.408\nabla\left(R_{\mathrm{n}} - G\right) + \gamma\frac{900}{T+273}U_2\left(e_{\mathrm{s}} - e_{\mathrm{a}}\right)}{\nabla + \gamma\left(1 + 0.34U_2\right)}. \quad (1)$$

Next, the difference between month-by-month precipitation and evapotranspiration was calculated by the formula:

$$D_i = P_i - PET_i. \quad (2)$$

Based on the PET and precipitation from GCM data, the log-logistic probability distribution was used to fit the difference between precipitation and PET, and the SPEI value corresponding to each D_i value was calculated. By applying the same parameters of distribution function established in the historical period 1961–2015, the SPEI dryness/wetness conditions in future can be assessed. When the cumulative probability $P < 0.5$, the SPEI is calculated as:

$$w = \sqrt{-2\ln\left(P\right)} \quad (3)$$

$$\mathrm{SPEI} = w - \frac{c_0 + c_1 w + c_2 w^2}{1 + d_1 w + d_2 w^2 + d_3 w^3} \quad (4)$$

where: $d_1 = 1.432788$; $d_2 = 0.189269$; $d_3 = 0.001308$; $c_0 = 2.551517$; $c_1 = 0.802853$; and $c_2 = 0.010328$.

However, when $P > 0.5$, the SPEI is calculated as:

$$\mathrm{SPEI} = -\left(w - \frac{c_0 + c_1 w + c_2 w^2}{1 + d_1 w + d_2 w^2 + d_3 w^3}\right). \quad (5)$$

2.2.2. Identification of drought events

The run theory first proposed by Yevjevich (1969) is widely used to identify and characterize different droughts events (Yevjevich 1969). A run is the portion of all values in a time series that is below or above a cutoff threshold. The portion below the cutoff threshold is a negative tour, while the opposite part is a positive tour. According to the definition of drought events by McKee *et al* (1993), we determine it by the following three criteria: The SPEI value is consistently less than 0, then the minimum SPEI value during the period is less than −1, lastly, the total duration is greater than or equal to 3 months. The persistent low intensity drought events can also have a significant impact on agriculture, vegetation growth, and local ecosystems as well as high intensity drought events (Guo *et al* 2018). Therefore, the run theory was used to identify these two types of droughts events comprehensively.

To study future drought events characteristics and quantify the development of future drought, this paper compares the historical period of 1960–2000 with the SPEI values for the two time periods 2021–2060 and 2061–2100. As well, it combines the run theory to extract drought events and describe their basic characteristics, including drought frequency (DF), mean drought duration (MDD), and mean drought intensity (MDI). The differences in multi-year drought characteristics between the two stated time periods were also calculated to analyze the differences in drought characteristics between these periods, expressed as relative DF, relative MDD, and relative MDI. Drought events intensity was calculated by computing the average of the intensity of all drought events on each grid during the reference period and the two future periods. When calculating the three attributes of the average drought event over global land, we assumed that for each grid cell, for each model and SSP, a series of drought events are identified based on run theory. Therefore, the attributes of each event are calculated. The attributes are then averaged over all grid cells, all models, and all SSP scenarios for each 40 year period.

3. Results

3.1. Comparison of GCM simulated data with observed data

The Taylor diagram is an effective method for model evaluation and testing. We use Taylor diagrams to compare models visually. From figure 1 we can see that GCM can simulate changes in temperature very well. Further, the correlation coefficients of all nine GCMs are greater than 0.99, which is quite close to 1. The standard deviation indicates the ability of the GCM to simulate the center amplitude. The standard deviation of the nine GCMs is uniformly distributed around 1 and they have excellent performance in the simulation of the center amplitude. The root mean square error is used to measure the deviation of the observations from the GCM and is less than 0.13 for all nine GCMs.

The simulation of GCMs for precipitation is not as competently as that for temperature, Other than for FIO-ESM-2-0, the correlation coefficients between GCMs and measured data are distributed between 0.72 and 0.89. Regarding the ability to simulate the central amplitude, the standard deviation of GCM is generally small overall, with a standard deviation of less than 1. This indicates a weak simulation of the precipitation amplitude. Among them, ACCESS-CM2 has the best performance with a standard deviation value of 1.04. In contrast, FIO-ESM-2-0 has the smallest standard deviation of 0.40. Regarding deviations between observations and GCMs, the root means square error values of the nine GCMs were distributed between 0.47 and 0.85, with the smallest deviation for IPSL-CM6A-LR and the largest deviation for FIO-ESM-2-0.

The GCMs performed well for the simulation of PET, which illustrates the precision of the

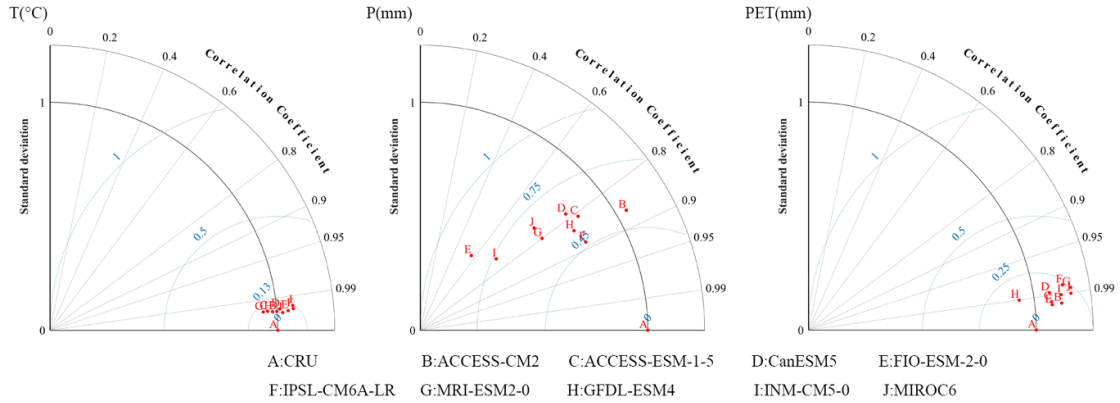

Figure 1. Standardized Taylor diagram showing model simulation capability of simulated values for nine GCMs from 1950 to 2015 for observation data of temperature, precipitation, and potential evapotranspiration. (Standard deviation in Standardized Taylor diagram is the ratio of the standard deviation of model to the standard deviation of observations).

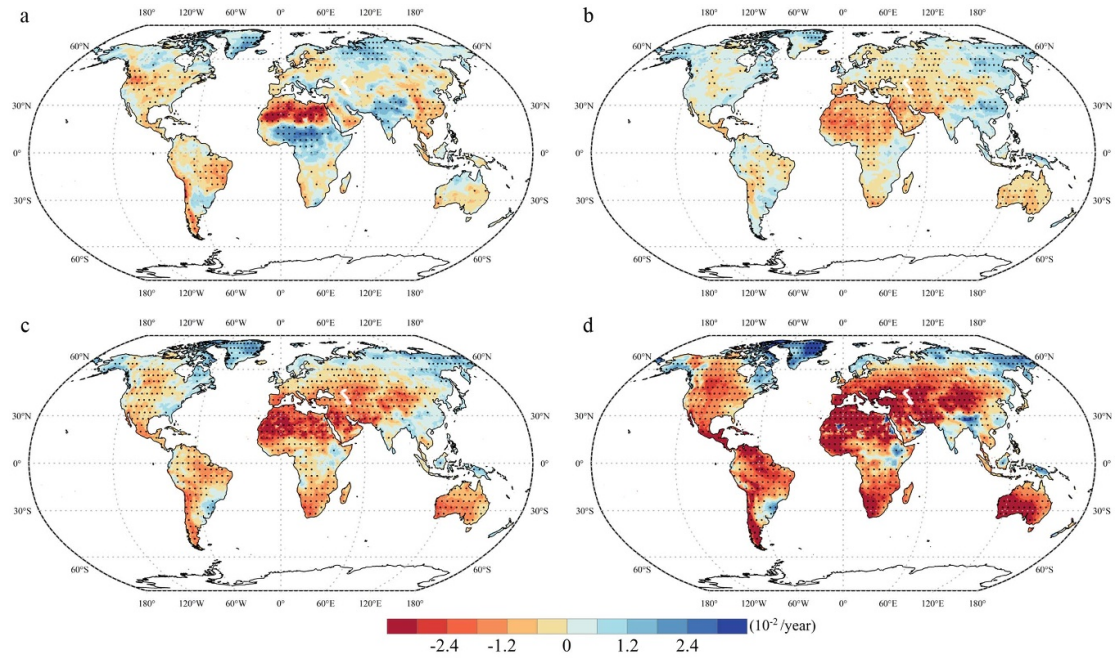

Figure 2. Spatial distribution of estimated Sen's slope of monthly SPEI values for the historical period (a) and three future paths of SSP126 (b), SSP245 (c) and SSP585 (d). The dot in the figure indicates that the region exceeds the Mann–Kendall significance test (0.05).

Penman–Monteith formula for calculating PET. The correlation coefficients in all nine GCMs were greater than 0.98, with high correlation. The overall performance is good in terms of the ability to simulate the center amplitude, and it can simulate the amplitude accurately. Except for the standard deviation of GFDL-ESM4, which is less than 1, the standard deviation of other GCMs is slightly larger than 1. Regarding the deviation between observations and GCMs, the root mean square error was less than 0.25 for all nine GCMs.

3.2. Future trend changes of drought

We analyzed the spatial distribution characteristics of global drought change trends based on Sen's slope of drought trends and MK significance test with a 0.05 significance level. In terms of spatial distribution, the spatial pattern of future drought change in the lower SSP126 is consistent with the medium SSP245 and the higher SSP585, while the spatial distribution of dry and wet change trends is relatively concentrated and well-defined. The distribution is also relatively concentrated and well-defined. In figure 2, the regions of intensifying drought are mainly concentrated in Australia, Middle East, South Africa, the Amazon basin, North Africa, Europe and Central Asia. These are mostly arid regions, indicating that in the context of climate change, the decrease in precipitation and the increase in potential evapotranspiration in the global arid regions in the future may lead to further intensification of drought in arid areas.

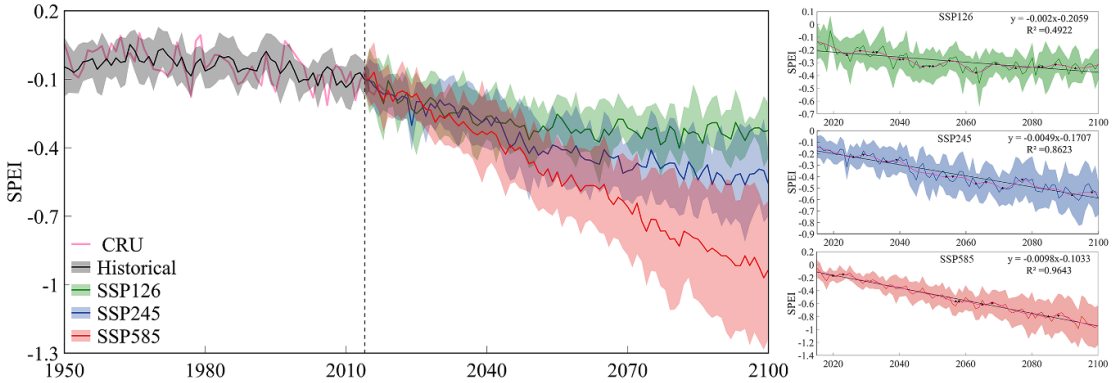

Figure 3. Temporal evolution of SPEI on a 12 month scale for global land and three future paths SSP126, SSP245 and SSP585 and the color lines represent the SPEI by ensemble mean of GCMs in 2015–2100 under SSPs. The shadow represents the range of multiple GCMs. The black dashed line indicates the year 2015, allowing a better comparison between the historical period and the future period, the linear trend line (information corresponding to the linear trend line is given in the upper right corner) and the smoothed line based on local regression (LOESS) and spanning 15 years are fitted on the right side and marked with black and magenta solid lines, respectively. The corresponding black triangle is the turning point based on the LOESS curve.

In the case of SSP126, the magnitude of change is smaller and less stable. The percentage of global land area that exceed the 0.05 significance test under the SSP126 was 47.4%, the percentage of global land area that exceed the 0.05 significance test and showed drought intensification was 36.2%, in arid and semi-arid regions, 67.0% of the regions indicated droughts intensify significantly. In the case of the high scenario (SSP585), the variation is large and shows substantial drought intensification. Globally, 85.7% of the land surface exceed the 0.05 significance test, the percentage of the global land regions indicated droughts intensify significantly was 68.2%, in arid and semi-arid regions, 93.2% of the regions indicated droughts intensify significantly. This suggests that some changes in future drought can be mitigated by reducing greenhouse gas (GHG) emissions, especially when the lower emission SSP is compared to the medium emission scenario SSP245. In the latter scenario, 68.3% of the global land surface exceed the 0.05 significance test, the model data exceed the 0.05 significance test, and the percentage of global land area exhibiting increased drought is 53.3%, in arid and semi-arid regions, 90.5% of the regions indicated droughts intensify significantly. It is clear that the magnitude of change is skewed toward future changes in higher SSP, which is further strong evidence of the need to control GHG emissions. However, even at lower emissions, strong changes are expected in many regions, especially in Australia, the Amazon, and Central Asia.

The results indicate an overall decreasing trend in global wet and dry variability for the period 2015–2100, with droughts intensifying over time. Meanwhile, in figure 3, the SPEI values for the three future SSPs show dramatic differences in development after 2060. The risk of drought intensification is higher in Australia, South Africa, the Amazon basin, North Africa, Europe, and Central Asia.

3.3. Projections of the drought events characteristics

3.3.1. Duration of drought events

The spatial pattern of drought events duration changes relative to the historical period in two different study time periods and three future SSPs is shown in figure 4. As can be seen, the increase in drought events duration is greater in the dry zone under the high-emissions shared socioeconomic path. In contrast, the drought events duration in the wet zone exhibits a slight increase, with the wet zone with a larger value of drought events duration increase mainly located in the Amazon River basin. It is worth noting that, while under the high emission SSPs, European regions also exhibit an increase in drought events duration.

This increase is also evidenced by the mean drought events duration in the global terrestrial humid and semi-humid regions and in the arid and semi-arid regions. The average drought events duration over global land is estimated to be 4.4 months, 5.7 months, and 8.6 months (average of all SSP scenarios) corresponding to the historical periods 1960–2000, 2021–2060, and 2061–2100, respectively. In arid and semi-arid areas, the estimated durations are 6.5, 9.5, and 15.3 months, respectively, whereas in humid and semi-humid areas, there is a slightly increase in the trend of drought events duration to 3.6, 4.3, and 5.7 months, respectively. It should be emphasized that drought events with longer durations are expected to be particularly prominent during 2061–2100, especially in arid and semi-arid regions. For comparisons between shared SSPs in terms of emission effects, longer drought events duration corresponds to higher emission SSPs. This correspondence is mostly concentrated in drought regions in the latter two periods and is more pronounced in 2061–2100. In the Amazon and European regions, this phenomenon is also more pronounced

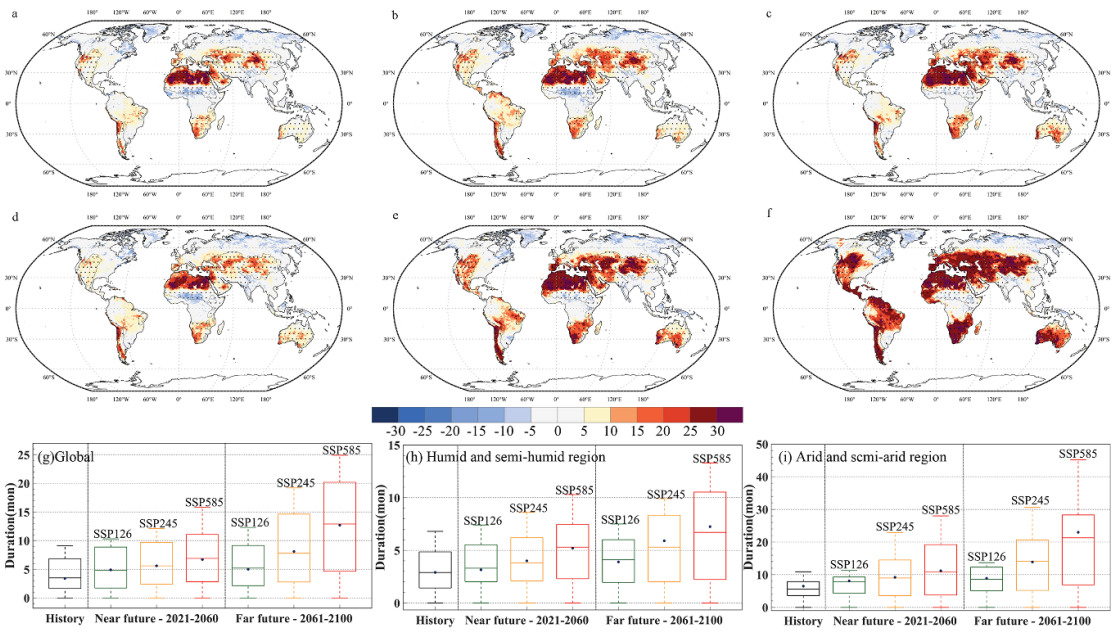

Figure 4. Spatial distribution of relative drought event duration in global terrestrial for two future cycles 2021–2060 (a)–(c), 2061–2100 (c), (d), (f) under SSP126 (a), (d), SSP245 (b), (e) and SSP585 (c), (f) scenarios, relative to the reference cycle 1961–2000. The dotted regions indicate the eight global arid regions: Middle East Asia, Southwest Asia, Sahara (North Africa and Sahara Desert), Horn of Africa, South Africa, Australia, southwest USA, and Patagonia (same as sections 3.3.2 and 3.3.3). Changes in the duration of drought events over the periods 2021–2060, 2061–2100 identified by the SPEI, represented by box plots, distinguishing global (g), humid and semi-humid regions (h) and arid and semi-arid regions (i), relative to the reference SSP126, SSP245, SSP585 scenarios. The box plots and the black dots denote the five statistics: minimum, first quartile, median, third quartile with maximum and mean, respectively.

during the same period, with estimated future durations of 3.7, 5.3, and 9.8 months, respectively, in the European region, and distribution corresponding to SSP126, SSP245, and SSP585. In contrast, in the Amazon basin, the estimated future durations are 3.5, 4.8, and 9.1 months, respectively. Overall, these two regions face a high risk of drought under high emission scenarios. Notably, when considering all pathways, regions and future periods, the high emission scenario SSP585 consistently exhibits a longer duration.

3.3.2. Frequency of drought events

The drought events frequencies were calculated for each grid for the reference and future periods (frequencies are events per 40 years). Relative to the reference period, changes in the spatial pattern of drought events frequencies are expected to be manifested in different periods and scenarios primarily in the United States, the Amazon basin, the Sahara, Australia, South Africa, Europe, and Central Asia (figure 5). The decreasing trend in drought events frequency which occurs mainly in the Sahara and the South Asian peninsula is caused by the shift from drought events to long-term drought events in the Sahara.

The average global drought events frequency for all regions is estimated to be about 12.7 and 11.8 events (average of all scenarios), respectively, which is higher than the reference cycle of 9.1 events for the future periods 2021–2060 and 2061–2100. Therefore, the frequency of future drought events will be higher relative to the reference period.

The average frequency of drought events in arid and semi-arid regions is 15.5 and 11.9, respectively, and the frequency of long-term drought events in arid regions will decrease during 2021–2060 and 2061–2100. However, the duration of drought events will increase with the intensity of drought, which indicates that drought events in arid regions will turn into stronger drought. Unlike the arid and semi-arid regions, the change in drought events frequency in humid and semi-humid regions will increase insignificantly 11.3 and 11.8 times during 2021–2060 and 2061–2100, respectively.

When comparing SSPs in terms of emission effects, lower DF corresponds to higher emission SSPs. For the next two periods, this correspondence is mostly concentrated in drought regions, with drought frequencies of 16.5, 15.5, and 14.2 during 2021–2060 and distribution corresponding to SSP126, SSP245 and SSP585. This relationship is more obvious during 2061–2100, at 14.4, 12, and 9.3 times, respectively. Combined with the above analysis of drought ephemeris, this further indicates that drought events in the arid zone will transform into long-term drought events under high emission SSPs.

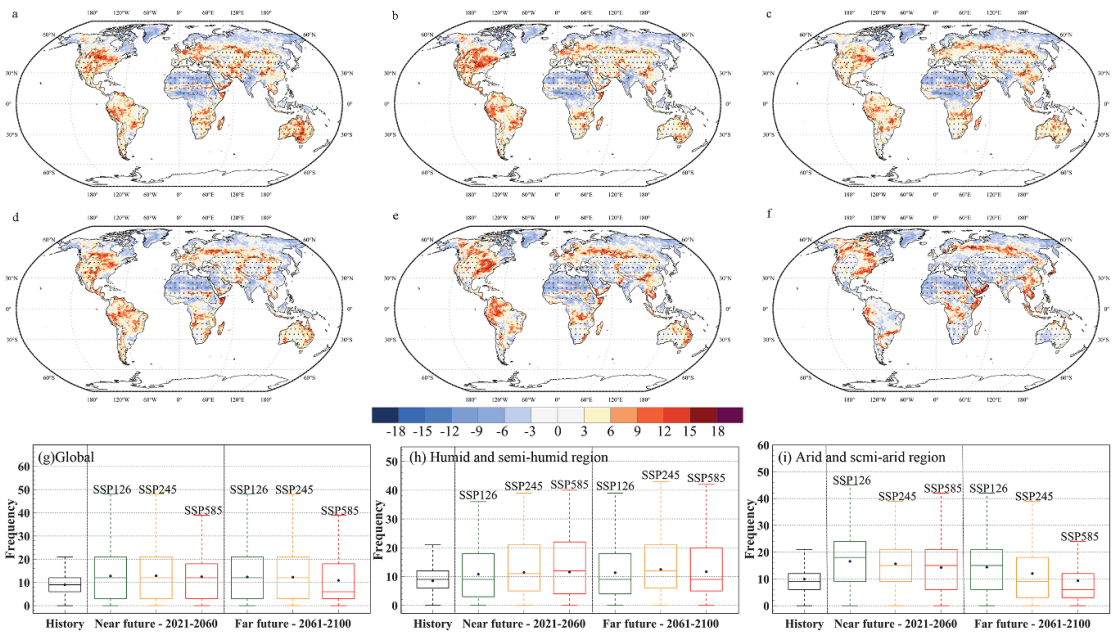

Figure 5. Spatial distribution of relative drought event frequency in global terrestrial for two future cycles 2021–2060 (a)–(c), 2061–2100 (c), (d), (f) under SSP126 (a), (d), SSP245 (b), (e) and SSP585 (c), (f) scenarios, relative to the reference cycle 1961–2000.
Changes in the frequency of drought events over the periods 2021–2060, 2061–2100 identified by the SPEI, represented by box plots, distinguishing global (g), humid and semi-humid regions (h) and arid and semi-arid regions (i), relative to the reference SSP126, SSP245, SSP585 scenarios. The box plots and the black dots denote the five statistics: minimum, first quartile, median, third quartile with maximum and mean, respectively.

3.3.3. Intensity of drought events

Drought event intensity was calculated as the 40 year average of all event-average SPEI values at each grid cell for each of the periods of interest (averaged over all models). Figure 6 shows the absolute change in drought events intensity between the future period and the reference year. Relative to the reference period, nearly all mid- and low-latitude regions of the globe exhibit an increase in drought events intensity for almost all SSP scenarios and future periods. The projected results indicate that relatively large increases in drought events intensity are concentrated in western United States, Patagonia, Sahara, Middle East, South Africa, Central Asia, and Australia, and that drought events intensity and spatial patterns will be very similar in the three climate scenarios during the future period 2021–2060. Drought events intensity will increase significantly in European region and Amazon River basin during 2061–2100 under SSP245 and SSP585. Moreover, the intensity and duration of droughts will be decreased in the higher latitudes of the northern hemisphere, such as Iceland and northern Siberia.

The regional average drought events intensity over the global land surface during the reference period is estimated to be −0.62. However, severe drought events are expected to occur in the future according to the model. Specifically, in 2021–2060 and 2061–2100, the intensity is anticipated to be −0.75 and −0.97 (all SSP averages), respectively.

In both humid and arid areas, although the spatial pattern of drought events intensity change is consistent (as shown in figure 6), the average expected drought events intensity in arid areas is more significant than that in arid and semi-humid areas. In 2021–2060, the drought events intensity in arid areas is expected to be −1.1, while that in wet areas is expected to be −0.58. Meanwhile, in 2061–2100, the intensity is estimated to be −1.5 in arid areas and −0.67 in wet ones. The difference between arid and wet areas is further widened in the late 21st century, when arid areas suffer from even more severe drought consequences. Furthermore, in terms of changes in intensity levels under climate scenarios, the projections show that more severe droughts events are likelier to occur globally under higher emission scenarios, especially in the late 21st century, with global drought events intensity reaching −1.21 under the SSP585 emission scenario and even −2.0 (extreme drought) in arid regions.

4. Discussion

4.1. Drylands at greater risk

By the end of this century, arid areas are expected to cover half of the global land surface, with increased warming and population growth, drylands in developing countries will experience degradation and desertification (Huang *et al* 2016). Arid areas

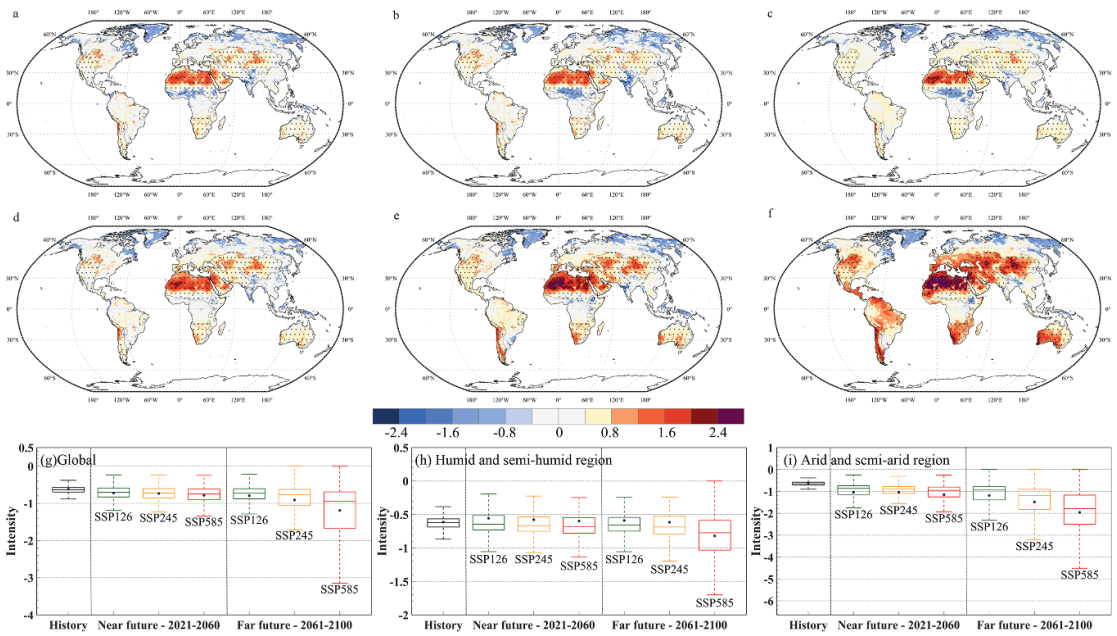

Figure 6. Spatial distribution of relative drought event intensity in global terrestrial for two future cycles 2021–2060 (a)–(c), 2061–2100 (c), (d), (f) under SSP126 (a), (d), SSP245 (b), (e) and SSP585 (c), (f) scenarios, relative to the reference cycle 1961–2000.
Changes in the intensity of drought events over the periods 2021–2060, 2061–2100 identified by the SPEI, represented by box plots, distinguishing global (g), humid and semi-humid regions (h) and arid and semi-arid regions (i), relative to the reference SSP126, SSP245, SSP585 scenarios. The box plots and the black dots denote the five statistics: minimum, first quartile, median, third quartile with maximum and mean, respectively.

(drylands) are more sensitive and vulnerable to climate change than wet areas (wetlands), and there are large asymmetries in response. Previous studies have reported that the magnitude of climate change in global drylands will exceed the global average (Huang *et al* 2017). Due to global warming, some borders of wetlands will be transformed into drylands, and that more severe droughts will occur in these new drylands (Feng and Fu 2013, Sherwood and Fu 2014, Berg *et al* 2016).

Our study is based on drylands as defined by historical data, investigated regional differences in future changes of drought, arid areas face more severe drought threats compared to wet areas, and wet areas will be transformed into arid areas, which in return will negatively affect more people's lives. Drought will pose greater challenges to agriculture, water management, and human health in arid regions. The findings indicated that by the late 21st century, drought events duration will be 2.7 times longer and drought events intensity 2.2 times more severe in arid areas than in wet ones under the SSP585 path. The cause of this difference may be due to plant transpiration against photosynthesis (Liu *et al* 2006), where the physiological response of plants under conditions of high CO_2 reduces the prediction of future drought stress (Swann *et al* 2016). Other factors include the effect of clouds and aerosols on energy balance (Huang *et al* 2017). Therefore, when conducting global warming studies, anticipated future changes in arid regions and regional differences cannot be ignored.

4.2. Addressing future drought risks

Based on the three typical SSPs in CMIP6, this study used the Penman–Monteith formula with SPEI indicators to predict future drought conditions globally. The results showed that the magnitude and extent of drought increased significantly with increasing SSPs and warming, which suggests that future drought risk in hotspots can be mitigated by reducing GHG emissions.

Our model projections indicate a general trend towards drier global wet and dry variability, with droughts intensifying over time. The spatial distribution shows a higher risk of increased drought in Australia, South Africa, the Amazon Basin, North Africa, Europe and Central Asia. Our results further validate the risk of future drought. The global warming will increase the risk and severity of droughts in most subtropical and mid-latitude regions (Cook *et al* 2018). Severe and widespread droughts will occur worldwide over the next 30–90 years due to reduced precipitation and/or increased evaporation (Dai 2013), with drier average conditions, the risk of the most extreme drought events in history has increased with warming, by 200%–300% in some areas (Cook *et al* 2020). Specifically, the regional average drought event intensity over the reference period is estimated to be −0.62 over global land, while under the SSP585

scenario for 2061–2100, the intensity is projected to reach −1.19. Moreover, if contemporary rates of warming continue, water supplies and demand deficits could increase fivefold in Africa, Australia, southern Europe, south-central United States, Central America, the Caribbean, and parts of northwestern and southern China (Naumann *et al* 2018). Agricultural focus areas (Chile, Central Europe, Eastern United States and parts of China) and densely populated areas (e.g. Mediterranean. Southern Africa, Western Africa and southern North America) will suffer from more severe droughts, threatening water and food security (Ukkola *et al* 2020).

Europe and the Amazon basin region face more severe drought risks under the path of high emission SSPs, and future droughts in these two regions will break the balance of global socio-economic, agricultural production, and ecosystems, and further aggravating global warming (Webber *et al* 2018).

In the SSP585 scenario for 2061–2100, in the European region, the estimated future duration is 9.8 months and the intensity of drought is 2.8 times higher than in the historical period. Meanwhile, in the Amazon basin, the estimated future duration is 9.1 months and the drought intensity is 2.5 times higher than in the historical period. Overall, these two regions face a high risk of drought under the high emissions scenario. More than 82% of Europe's population is expected to live in urban areas by 2050 (UN Habitat 2011). The concentration of population, assets and activities makes it difficult for cities to adapt to increased droughts due to global warming (Shi *et al* 2016). At the same time, Central Europe is one of the major global food producers and exporters, and increased droughts could also threaten agricultural production in Europe.

Similarly, forest cover and evapotranspiration in the Amazon basin are crucial for the water cycle in tropical South America. Much of the basin will experience reduced rainfall in the future, especially in the eastern and southern parts of the Amazon, which will be dry in the 21st century (Parsons 2020). In addition, future changes in the region are particularly vulnerable to anthropogenic impacts on the region such as deforestation, land management, and forest fires (Nepstad *et al* 2014). Climate change will double the area burned by wildfires in the Amazon, and by 2050, 16% of the region's forests will be affected (Brando *et al* 2020). Drought and deforestation feedbacks will hinder efforts to curb drought and deforestation (Staal *et al* 2020). The combined stress-driven forest declines will in return have significant impacts on regional carbon sequestration (regional carbon sequestration), land degradation risk, biodiversity, and the global climate system. Therefore, to meet the challenges posed by future climate change, international cooperation is urgently needed for disaster management from the perspective of sustainable development of global human society.

5. Conclusion

The current analysis of the Coupled Model Intercomparison Project (CMIP) with the Intergovernmental Panel on Climate Change assessment report was our main source of data support and general information on how droughts will change in the future. Our study was based on the nine latest CMIP6 climate models, and we used the Penman–Monteith equation with SPEI to estimate future droughts under three SSPs (SSP126, SSP245 and SSP585). The results revealed that when emissions increase the global climate environment becomes drier and drought grow more severe and longer-lasting. Regions already classified as arid will suffer even more severe drought under high-emission SSPs. Specifically, 36.2% of global land will experience increased drought under SSP126, including 67.0% of regions currently designated as arid, with droughts intensifying significantly. Under SSP585, 68.3% of global land will suffer increased drought, with 93.2% of the arid regions experiencing significant drought intensification.

Furthermore, concerning to future droughts events, drought intensity will become more severe, drought duration will lengthen, and DF will decrease in arid regions, which indicates that drought events in arid regions will turn into severe drought. The duration of drought over global is estimated to be 4.4 months, 5.7 months, and 8.6 months for the time periods 1960–2000, 2021–2060, and 2061–2100, respectively. Notably, for the SSP585 scenario, by the late 21st century, drought events duration will be 2.7 times longer and drought events intensity 2.2 times more severe in arid regions than in humid regions, regions that are already arid may become universally drought-stricken. The most severe aridification trends will occur in the arid regions of Australia, Middle East, South Africa, the Amazon basin, North Africa, Europe, and Central Asia. In addition, Europe and the Amazon River Basin are also facing the threat of future drought. Increased aridification will put these regions and countries at risk of further land and ecological degradation, as well as increased poverty. The findings of this study have far-ranging implications not only for how we deal with the impacts of climate warming-induced drought disaster, but also for how these impacts affect socio-economic and ecological security.

Data availability statement

The data that support the findings of this study are available upon reasonable request from the authors.

Acknowledgments

The research is supported by the National Key Research and Development Program (2019YFA0606902) and the National Natural Science

Foundation of China (U2003302). The authors gratefully acknowledge the Youth Innovation Promotion Association of the Chinese Academy of Sciences (No. 2018480).

Competing financial interests

All authors reviewed the manuscript, and there is no competing financial interest.

References

Agel L and Barlow M 2020 How well do CMIP6 historical runs match observed Northeast U.S. Precipitation and extreme precipitation–related circulation? *J. Clim.* **33** 9835–48

Allen R G, Pereira L S, Raes D and Smith M 1998 *Table of Contents Originated by: Agriculture Crop evapotranspiration—Guidelines for computing crop water requirements—FAO irrigation and drainage paper 56*

Anon 2019 The CMIP6 landscape *Nat. Clim. Change* **9** 727

Berg A *et al* 2016 Land-atmosphere feedbacks amplify aridity increase over land under global warming *Nat. Clim. Change* **6** 869–74

Brando P M, Soares-Filho B, Rodrigues L, Assunção A, Morton D, Tuchschneider D, Fernandes E C M, Macedo M N, Oliveira U and Coe M T 2020 The gathering firestorm in southern Amazonia *Sci. Adv.* **6** 1–10

Chen H and Sun J 2015 Changes in drought characteristics over china using the standardized precipitation evapotranspiration index *J. Clim.* **28** 5430–47

Chen H, Sun J, Lin W and Xu H 2020 Comparison of CMIP6 and CMIP5 models in simulating climate extremes *Sci. Bull.* **65** 1415–8

Cook B I, Mankin J S and Anchukaitis K J 2018 Climate change and drought: from past to future *Curr. Clim. Change Rep.* **4** 164–79

Cook B I, Mankin J S, Marvel K, Williams A P, Smerdon J E and Anchukaitis K J 2020 Twenty-first century drought projections in the CMIP6 forcing scenarios *Earth's Future* **8** 1–20

Dai A 2013 Increasing drought under global warming in observations and models *Nat. Clim. Change* **3** 52–58

Di Luca A, Pitman A J and De Elía R 2020 Decomposing temperature extremes errors in CMIP5 and CMIP6 models *Geophys. Res. Lett.* **47**

Ding Y, Hayes M J and Widhalm M 2011 Measuring economic impacts of drought: a review and discussion *Disaster Prev. Manage.* **20** 434–46

Donohue R J, McVicar T R and Roderick M L 2010 Assessing the ability of potential evaporation formulations to capture the dynamics in evaporative demand within a changing climate *J. Hydrol.* **386** 186–97

EM-DAT 2021 The International Disaster Database (available at: https://www.emdat.be/index.php)

Feng S and Fu Q 2013 Expansion of global drylands under a warming climate *Atmos. Chem. Phys.* **13** 10081–94

Guo H, Bao A, Liu T, Jiapaer G, Ndayisaba F, Jiang L, Kurban A and De Maeyer P 2018 Spatial and temporal characteristics of droughts in Central Asia during 1966–2015 *Sci. Total Environ.* **624** 1523–38

Habitat U N 2011 *Cities and Climate Change: Global Report on Human Settlements 2011*

Harris I, Osborn T J, Jones P and Lister D 2020 Version 4 of the CRU TS monthly high-resolution gridded multivariate climate dataset *Sci. Data* **7** 1–18

Huang J, Yu H, Dai A, Wei Y and Kang L 2017 Drylands face potential threat under 2 °C global warming target *Nat. Clim. Change* **7** 417–22

Huang J, Yu H, Guan X, Wang G and Guo R 2016 Accelerated dryland expansion under climate change *Nat. Clim. Change* **6** 166–71

Kim Y H, Min S K, Zhang X, Sillmann J and Sandstad M 2020 Evaluation of the CMIP6 multi-model ensemble for climate extreme indices *Weather Clim. Extremes* **29** 100269

Li Z, Chen Y, Fang G and Li Y 2017 Multivariate assessment and attribution of droughts in Central Asia *Sci. Rep.* **7** 1–12

Liu Z, Notaro M, Kutzbach J and Liu N 2006 Assessing global vegetation-climate feedbacks from observations *J. Clim.* **19** 787–814

McKee T B, Doesken N J and Kleist J 1993 The relationship of drought frequency and duration to time scales *Proc. Eighth Conf. Appl. Climatol.* 179–84

Naumann G, Alfieri L, Wyser K, Mentaschi L, Betts R A, Carrao H, Spinoni J, Vogt J and Feyen L 2018 Global changes in drought conditions under different levels of warming *Geophys. Res. Lett.* **45** 3285–96

Nepstad D *et al* 2014 Slowing Amazon deforestation through public policy and interventions in beef and soy supply chains *Science* **344** 1118–23

Nie S, Fu S, Cao W and Jia X 2020 Comparison of monthly air and land surface temperature extremes simulated using CMIP5 and CMIP6 versions of the Beijing Climate Center climate model *Theor. Appl. Climatol.* **140** 487–502

Parsons L A 2020 Implications of CMIP6 projected drying trends for 21st century Amazonian drought risk *Earth's Future* **8** e2020EF001608

Ritchie J and Dowlatabadi H 2017 Why do climate change scenarios return to coal? *Energy* **140** 1276–91

Sheffield J, Wood E F and Roderick M L 2012 Little change in global drought over the past 60 years *Nature* **491** 435–8

Sherwood S and Fu Q 2014 A drier future? *Science* **343** 737–9

Shi L *et al* 2016 Roadmap towards justice in urban climate adaptation research *Nat. Clim. Change* **6** 131–7

Srivastava A, Grotjahn R and Ullrich P A 2020 Evaluation of historical CMIP6 model simulations of extreme precipitation over contiguous US regions *Weather Clim. Extremes* **29** 100268

Staal A, Flores B M, Aguiar A P D, Bosmans J H C, Fetzer I and Tuinenburg O A 2020 Feedback between drought and deforestation in the Amazon *Environ. Res. Lett.* **15** 44024

Su B *et al* 2020 Insight from CMIP6 SSP-RCP scenarios for future drought characteristics in China *Atmos. Res.* **250** 105375

Swann A L S, Hoffman F M, Koven C D and Randerson J T 2016 Plant responses to increasing CO_2 reduce estimates of climate impacts on drought severity *Proc. Natl Acad. Sci. USA* **113** 10019–24

Thorarinsdottir T L, Sillmann J, Haugen M, Gissibl N and Sandstad M 2020 Evaluation of CMIP5 and CMIP6 simulations of historical surface air temperature extremes using proper evaluation methods *Environ. Res. Lett.* **15** 124041

Trenberth K E, Dai A, Van Der Schrier G, Jones P D, Barichivich J, Briffa K R and Sheffield J 2014 Global warming and changes in drought *Nat. Clim. Change* **4** 17–22

Ukkola A M, De Kauwe M G, Roderick M L, Abramowitz G and Pitman A J 2020 Robust future changes in meteorological drought in CMIP6 projections despite uncertainty in precipitation *Geophys. Res. Lett.* **47** 1–9

Van Der Schrier G, Jones P D and Briffa K R 2011 The sensitivity of the PDSI to the Thornthwaite and Penman-Monteith parameterizations for potential evapotranspiration *J. Geophys. Res. Atmos.* **116** 1–16

Van Dijk A I J M, Beck H E, Crosbie R S, De Jeu R A M, Liu Y Y, Podger G M, Timbal B and Viney N R 2013 The Millennium Drought in southeast Australia (2001–2009): natural and human causes and implications for water resources, ecosystems, economy, and society *Water Resour. Res.* **49** 1040–57

Vicente-Serrano S M, Beguería S and López-Moreno J I 2010 A multiscalar drought index sensitive to global warming: the

standardized precipitation evapotranspiration index *J. Clim.* **23** 1696–718
Wang H, Chen Y, Pan Y and Li W 2015 Spatial and temporal variability of drought in the arid region of China and its relationships to teleconnection indices *J. Hydrol.* **523** 283–96
Wang Y *et al* 2019 Tens of thousands additional deaths annually in cities of China between 1.5 °C and 2.0 °C warming *Nat. Commun.* **10** 1–7
Webber H *et al* 2018 Diverging importance of drought stress for maize and winter wheat in Europe *Nat. Commun.* **9** 1–10
Wild M 2020 The global energy balance as represented in CMIP6 climate models *Clim Dyn* **55** 553–77
Yang J *et al* 2021 Projecting heat-related excess mortality under climate change scenarios in China *Nat. Commun.* **12** 1039
Yevjevich V 1969 An objective approach to definitions and investigations of continental hydrologic droughts *Hydrol. Pap.* **23** 1–18
Zhai J, Mondal S K, Fischer T, Wang Y, Su B, Huang J, Tao H, Wang G, Ullah W and Uddin M J 2020 Future drought characteristics through a multi-model ensemble from CMIP6 over South Asia *Atmos. Res.* **246** 105111
Zhang J, Sun F, Xu J, Chen Y, Sang Y F and Liu C 2016 Dependence of trends in and sensitivity of drought over China (1961–2013) on potential evaporation model *Geophys. Res. Lett.* **43** 206–13
Zhang Z, Chen X, Xu C Y, Hong Y, Hardy J and Sun Z 2015 Examining the influence of river-lake interaction on the drought and water resources in the Poyang Lake basin *J. Hydrol.* **522** 510–21